JOURNAL OF CATALYSIS 156, 208–218 (1995)

Structural and Surface Properties of $CuO–ZnO–Cr_2O_3$ Catalysts and Their Relationship with Selectivity to Higher Alcohol Synthesis

J. M. Campos-Martín,* A. Guerrero-Ruiz,† and J. L. G. Fierro*,[1]

*Instituto de Catálisis y Petroleoquímica, C.S.I.C., Campus UAM, Cantoblanco, 28049 Madrid, Spain; and
†Departamento de Química Inorgánica, U.N.E.D., Senda del Rey s/n, Ciudad Universitaria, 28040 Madrid, Spain

Received May 16, 1994; revised April 25, 1995; accepted May 12, 1995

A series of copper–zinc–chromium catalysts of different compositions and calcination temperatures has been prepared, characterized by several techniques (BET specific surface area, XRD, gravimetric TPR, TPD-CO, and XPS), and tested under high alcohol synthesis (HAS) conditions. CO hydrogenation was carried out at reaction temperatures of 523–598 K and 50 bar total pressure. The influence of catalyst composition, calcination temperature, and surface characteristics on the HAS selectivity was studied. The optimum HAS yields were found in the low Cr content region, but chromium was needed. Although chromium oxide does not seem to be involved in the catalytic site, its presence in the catalyst composition is essential, owing to the larger specific surfaces and catalyst stability obtained at the highest reaction temperatures. For low Cr content composition, the temperature-programmed reduction (TPR) profiles were shifted to higher temperatures and simultaneously larger CO_2 amounts were found in the temperature-programmed desorption profiles of adsorbed CO (TPD-CO). Photoelectron spectra (XPS) revealed that the oxidation state of copper is Cu^{2+} in the calcined catalysts and Cu^0 in the reduced ones; Cu^+ was only stabilized in a $CuCr_2O_4$ spinel in the Cr-rich catalysts. These features derived from catalyst characterization are discussed in the framework of the catalytic behaviour for HAS synthesis. © 1995 Academic Press, Inc.

INTRODUCTION

Methanol synthesis from $CO/CO_2/H_2$ mixtures is an extremely useful technological option that has been explored for many years and developed on the industrial scale by ICI. Although there are excellent reviews (1–7) on this subject covering the general aspects of the catalysts and processes, more specific problems relevant to industrially important methanol synthesis ternary oxide $CuO–ZnO–MeO_x$ catalysts have also been reviewed (8–14). In the last decade the chemical and petrochemical industries have shown renewed interest in the use of methanol and higher aliphatic alcohols. The reasons for this lie in: (i) decreasing the dependence on oil by synthesizing alternative clean fuels from synthesis gas ($CO + H_2$), which can be obtained from natural gas (15) or coal (16), which are more abundant carbon sources than oil; (ii) using alcohols to synthesize other oxygenates such as methyl-tert-butyl ether (MTBE) as high octane blending stock for gasoline. Points (i) and (ii) are fulfilled by high molecular weight alcohols. Thus, isobutanol instead of MTBE could be used as an additive for gasolines, the production of the latter being almost restricted to FCC units and steam crackers. Another incentive for incorporating oxygenates in liquid fuels lies in the general acceptance of more restrictive new regulations for the reformulated gasolines. As the combustion of oxygenates reduces the level of contaminants in the exhaust (17), an interesting option would be to incorporate higher alcohols into gasoline because a mixture of branched C_1 to C_6 alcohols possesses ROM values and properties (18, 19), and price (20), similar to the more conventional MTBE additive. As a liquid fuel, methanol displays several advantages: (i) low price, like gasolines; (ii) CO, NO_x, and unburned hydrocarbons emissions are lower than gasolines; (iii) its chemical properties lead to more efficient combustion. However, it still suffers from incomplete combustion with the subsequent emission of traces of formaldehyde (22). Without doubt the principal problem resides in the engine itself, which is designed to operate with gasoline but not with methanol. In California, a strategic plan has been put into practice to slowly increase the proportion of methanol until the full replacement of gasoline in fifteen years time (23). As this use of methanol suffers from the increased solubility of water up to unacceptable levels, the substitution of methanol by higher alcohols appears very promising (24). Accordingly, many recent activities in synthesis gas conversion deal with the higher alcohol synthesis (HAS).

Considerable disagreement exists in the literature concerning the valence state of copper in the sites of Cu–Zn–Me–O systems possessing the requisite activity and selec-

[1] To whom correspondence should be addressed.

0021-9517/95 $12.00

tivity for CO hydrogenation under typical reaction conditions, namely, 50–100 bar overall pressure and 500–570 K for reaction temperature. The broad range of disagreement may be appreciated by noting that research groups have argued for a central role of metallic Cu^0 sites in activating hydrogen and for a close relationship between copper metal area and activity in methanol synthesis (25–29), while others have argued for a central role of Cu^+ ions dispersed in the zinc oxide phase in the adsorption and activation of carbon monoxide (9, 30–33). Besides that, EXAFS studies appear controversial because several authors found no evidence on the stabilization of Cu^+ ions (34–36), whereas the stabilization of Cu^- within the ZnO lattice has been recently documented by others (37–39). Moreover, the HAS seems to occur from methanol according to the equation ($2CH_3OH \rightarrow C_2H_5OH + H_2O$) (40) and by adding intermediate C_1 oxygenates to the alcohol molecule (41). The coupling of methanol molecules and/or addition of C_1 species in the alcohol chain appears to be inhibited by the presence of CO_2 in the feed.

Our intention in undertaking this work was to concentrate attention upon the selection of the optimal composition of the Cu–Zn–Cr–O catalysts, which yield the maximum HAS products from syngas, by making detailed comparisons of catalytic performances.

EXPERIMENTAL

Catalyst Preparation

The catalysts used in this study were prepared following the coprecipitation method (30, 42). For such a purpose, to an aqueous solution of the copper, zinc, and chromium nitrates of appropriate concentration a 0.5 *M* ammonium bicarbonate (all Merck reagent grade) solution was added until a final pH close to 7.5 was reached. After filtration, the precipitate was repeatedly washed, to remove the major fraction of adsorbed NH_4^+, CO_3^{2-}, and NO_3^- ions, and dried at 393 K. The dry precursors were then calcined in air at either 673 or 553 K (samples denoted by B) for 24 h. The final composition was obtained by atomic absorption spectrometry. The calcined catalysts were subsequently pelleted, ground, and sieved to particle sizes of 0.59–0.42 mm. For the sake of simplicity, the catalysts will be referred to hereafter as xCuyZnzCr, where x, y, and z denote the molar percentage of copper, zinc, and chromium elements, respectively. The catalyst calcined at low temperature will be denoted by the same nomenclature but adding B at the end.

Experimental Techniques

X-ray diffraction patterns were recorded from both calcined and used catalysts using a Seifert 3000P vertical diffractometer and nickel-filtered Cu$K\alpha$ radiation ($\lambda = 0.1538$ nm), under constant instrumental parameters. For each sample, Bragg angles between 5° and 75° were scanned at a rate of 2°/min. Specific surface areas of the catalysts were calculated by applying the BET method to the N_2 adsorption isotherms, measured at liquid nitrogen temperature on a Micromeritics ASAP 2000 equipment, and taking a value of 0.162 nm^2 for the cross section of the adsorbed nitrogen molecule.

Temperature-programmed reduction (TPR) experiments were carried out in a Cahn 2000 microbalance working at a sensitivity of 10 μg. The reduction process was followed by monitoring the weight loss of the sample. The samples (5–10 mg) were heated in a flow of helium (99.999 vol%) (60 ml/min) up to 473 K in order to remove adsorbed water and other gaseous contaminants. Following cooling to room temperature in the same flow of helium, a switch was made to a mixture of 2 vol% hydrogen (99.995 vol%) in helium (60 ml/min) and again heated at a rate of 4 K/min up to 673 K while the weight changes were continuously recorded. The microbalance was interfaced to a microcomputer, which allowed accumulation and processing of weight change temperature curves.

Temperature-programmed desorption (TPD) experiments were performed on aliquots of catalyst (70 mg) placed in a quartz reactor attached to a vacuum line and gas-handling system. The samples were reduced in hydrogen at 473 K for 2 h and then outgassed at 10^{-5} Torr (1 Torr = 133.33 N/m^2) for 1 h at the same temperature. Subsequently, they were cooled down to room temperature and exposed to a CO pulse for 30 min. Once the gas phase was removed, the samples were heated to 673 K at a constant heating rate of 4 K/min. A Balzers QMG 125 quadrupole mass spectrometer, capable of monitoring 16 masses simultaneously, connected in line with the reactor, was used for the analysis of the desorption products.

Photoelectron spectra were acquired with a Fisons ESCALAB MkII 200R spectrometer equipped with a hemispherical electron analyzer and a Mg$K\alpha$ ($h\nu = 1253.6$ eV, 1 eV = 1.602×10^{-19} J) 120 W X-ray source. A PDP 11/04 computer from Digital Equipment Co. was used for collecting and analyzing the spectra. The powder samples were pressed into small aluminum cylinders and then mounted on a sample rod placed in a pretreatment chamber and heated under vacuum at 373 K for 1 h prior to being moved into the analysis chamber. After analysis, the same catalyst sample was moved to the pretreatment chamber and reduced *in situ* by hydrogen at 423, 523, and 623 K. The pressure in the ion-pumped analysis chamber was below 3×10^{-9} Torr during data acquisition. The spectra were collected for 20 to 90 min, depending on the peak intensities, at a pass energy of 20 eV, which is typical of high resolution conditions. The intensities were estimated by calculating the integral of each peak after the

smoothing and subtraction of the S-shaped background and the fitting of the experimental curve to a mixture of Lorentzian and Gaussian lines of variable proportion. All binding energies (BE) were referenced to the adventitious C 1*s* line at 284.9 eV. This reference gave BE values within an accuracy of ±0.2 eV.

Activity Measurements

The activity tests were carried out using a semiautomatic high-pressure fixed-bed catalytic reactor. The reactor was a 7 mm i.d. U-shaped titanium (grade 3) tube. The catalyst (1.5 g) was held in place in the middle of the second arm, the leading arm serving as a preheater. A chromel-alumel thermocouple placed on the outer wall of the reactor near the catalyst bed was used to measure and control the reactor temperature. The composition of the feed stream, CO (69 vol%) and H_2 (31 vol%), was adjusted by electronic mass flow controllers (Unit) to yield a spatial velocity of 3200 l(SPT)/kg_{cat} · h. The reaction was conducted to 50 bar overall pressure and reaction temperatures of 523, 548, 573, and 598 K with on-stream times of 20 h at each temperature. The effluents of the reactor were analyzed on line by GC. To avoid condensation of the reaction products, the outlet of the reactor was heated to 423 K. A Hewlett Packard 5890 Series II gas chromatograph equipped with Poraplot Q (25 m, 0.75 mm o.d.) and 5A molecular sieve (10 m, 0.75 mm o.d.) capillary columns was used for product separation. The analysis of the products was carried out with thermal conductivity (TCD) and flame ionization (FID) detectors which cover the analysis of CO, CO_2, and C_1–C_6 hydrocarbons, and C_1–C_5 alcohols.

RESULTS AND DISCUSSION

Surface Areas

The BET areas of the calcined catalysts are compiled in Table 1. From these results, it is evident that the BET areas for the binary (54Cu46Zn and 64Cu36Cr), and more specifically for the ternary (xCuyZnzCr) systems are much larger than those for the single oxides. This effect is more clear for the Cr-containing catalysts even in the region of low chromium contents. On the other hand, the precursors calcined at 553 K yield BET areas substantially higher than those calcined at 673 K. Moreover, the N_2 adsorption isotherms at 77 K show that samples calcined at 553 K have higher contributions of mesoporosity, which was detected by the larger quantities of N_2 adsorbed between relatives pressures 0.1 and 0.7.

X-Ray Diffraction

Bulk structures in both calcined and used catalysts have been revealed by XRD. The crystalline phases detected by XRD on calcined and H_2-reduced and used catalysts are compiled in Table 1. The fresh catalysts show diffraction lines of CuO and ZnO individual oxides and $ZnCr_2O_4$, whereas those used in CO hydrogenation display only ZnO and $ZnCr_2O_4$ phases and metallic Cu. This is due to the relative ease with which CuO becomes reduced at typical reaction temperatures and in the CO + H_2 environment. $CuCr_2O_4$ spinel is found in the binary and ternary chromium-rich catalysts. This phase can still be observed in the catalysts after use on-stream due to its high stability in a reducing atmosphere. Finally, poorly crystalline oxides are obtained upon calcination at 553 K, as revealed by the observation of broad and low intense diffraction peaks of CuO and ZnO in calcined samples or metallic Cu and ZnO in reduced counterparts, which contrasts with the intense and narrow peaks recorded for their homologues calcined at higher temperatures.

Temperature-Programmed Reduction

TPR profiles are shown in Figs. 1A, 1B, and 1C. The figures show the weight loss as a function of temperature. Although mainly due to reduction of CuO to Cu, some weight loss is due to decomposition of hydroxycarbonate precursor residue. The arbitrary unit value of 100 corresponds to the limiting value expected for the weight loss due to reduction of the CuO component to Cu. The profiles show that the reduction temperature depends markedly on the catalyst composition. For the Zn-rich catalysts, the onset temperature for CuO reduction is higher, whereas the opposite is observed for the Cr-rich compositions. Extended TPR profiles for the Cr-rich catalysts reveal weight loss tails still continuing at temperatures above 673 K. As copper chromite was found on the XRD patterns of the Cr-rich compositions, and as this compound is more difficult to reduce than CuO, it is inferred that the tails at higher temperatures present with these catalysts can be ascribed to the reduction of copper chromite. For the catalysts calcined at 553 K (Fig. 1C) the weight loss considerably oversteps the stoichiometric reduction of CuO to Cu^0. This is due to marked overlapping of residual precursor decomposition and the reduction itself. Another interesting finding derived from the profiles in Fig. 1C is the evident retardation of catalyst reduction for samples calcined at 553 K compared to 673 K. This behaviour agrees with the findings of Sermon *et al.* (43–46), who showed that amorphous copper catalysts are reduced at substantially higher temperatures than the crystalline ones. The lower the calcination temperatures of the precursors, the higher the temperatures needed for catalyst reduction. As can be seen below, the retardation of copper reduction either by the formation of a rather stable copper chromite or by obtaining some poorly crystalline copper-containing

TABLE 1

BET Specific Surface Areas and Crystalline Phases in the Catalysts

Catalysts	S_{BET} (m^2/g)	Crystalline phases detected by XRD	
		Calcined	Tested
35Cu50Zn15Cr	41.5	CuO, ZnO, $ZnCr_2O_4$	Cu, ZnO, $ZnCr_2O_4$
64Cu21Zn15Cr	32.8	CuO, ZnO, $ZnCr_2O_4$	Cu, ZnO, $ZnCr_2O_4$
55Cu8Zn37Cr	43.5	CuO, $ZnCr_2O_4$, $CuCr_2O_4$	Cu, $ZnCr_2O_4$, $CuCr_2O_4$
38Cu41Zn21Cr	39.2	CuO, ZnO, $ZnCr_2O_4$	Cu, ZnO, $ZnCr_2O_4$
60Cu10Zn30Cr	42.7	CuO, $ZnCr_2O_4$	Cu, $ZnCr_2O_4$
36Cu7Zn57Cr	36.4	CuO, $ZnCr_2O_4$, $CuCr_2O_4$	Cu, $ZnCr_2O_4$, $CuCr_2O_4$
54Cu46Zn	12.3	CuO, ZnO	Cu, ZnO
64Cu36Cr	30.4	CuO, $CuCr_2O_4$	Cu
100Cu	6.1	CuO	Cu
100Cr	17.8	Cr_2O_3	Cr_2O_3
100Zn	0.4	ZnO	ZnO
35Cu50Zn15CrB	68.6	ZnO	Cu, ZnO
64Cu21Zn15CrB	68.2	CuO	Cu
55Cu8Zn37CrB	79.2	—	Cu

phase yields, in general, more selective catalysts for HAS from syngas.

Temperature-Programmed Desorption of CO (TPD-CO)

TPD profiles after CO adsorption on prereduced samples are displayed in Fig. 2. It can be observed that CO desorption occurs in a narrow temperature window (315–475 K) (Fig. 2A). In addition, surface reaction of CO yields CO_2 at temperatures above 375 K (Fig. 2B). The participation of the water–gas shift reaction as a source of CO_2 seems to be excluded as no molecular water (m/z = 18) was detected at significant levels. It is worth noting that chromium oxide alone gives rise only to the observation of CO, but never CO_2. However, both CO and CO_2 are observed among the desorption products upon CO adsorption on sample 64Cu36Cr. For the ternary oxides xCuyZnzCr the changes are dramatic. While a strong CO desorption, with very low amount of CO_2, is observed on sample 36Cu7Zn57Cr, practically all CO is desorbed as CO_2 from samples 38Cu41Zn21Cr and 63Cu22Zn15Cr, practically all CO is desorbed as CO_2 from samples 38Cu41Zn21Cr and 63Cu22Zn15Cr. From these results it appears that CO desorbs as such from chromium oxide, whereas from the other samples CO_2 is also evolved (Fig. 2B). This CO_2 can originate from strong interaction of the CO with surface oxygen atoms of ZnO (xCuyZnzCr catalysts) (47) or with the surface of $CuCr_2O_4$ (64Cu36Cr and 36Cu7Zn57Cr samples). Note that these two last

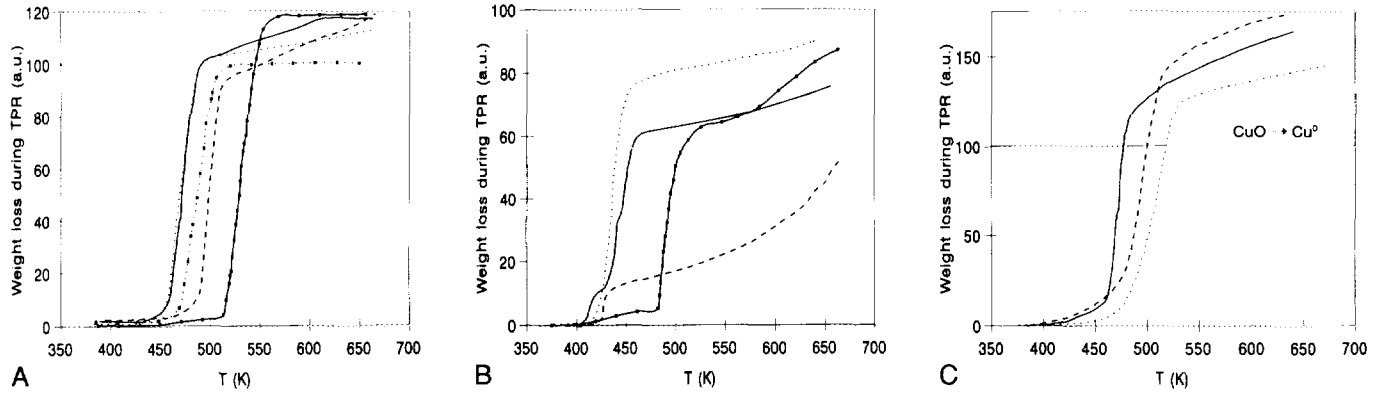

FIG. 1. (A) Temperature-programmed reduction (TPR) profiles for catalysts calcined at 673 K: (———) 35Cu50Zn15Cr, (···) 63Cu22Zn15Cr, (— —) 38Cu41Zn21Cr, (—■—) 54Cu46Zn, (·■·) 100Cu. (B) TPR profiles for catalysts calcined at 673 K: (———) 55Cu8Zn37Cr, (···) 60Cu10Zn30Cr, (— — 36Cu7Zn57Cr, (—■—) 64Cu36Cr. (C) TPR profiles for catalysts calcined at 553 K: (———) 35Cu50Zn15CrB, (···) 63Cu22Zn15CrB; (——) 55Cu8Zn37CrB.

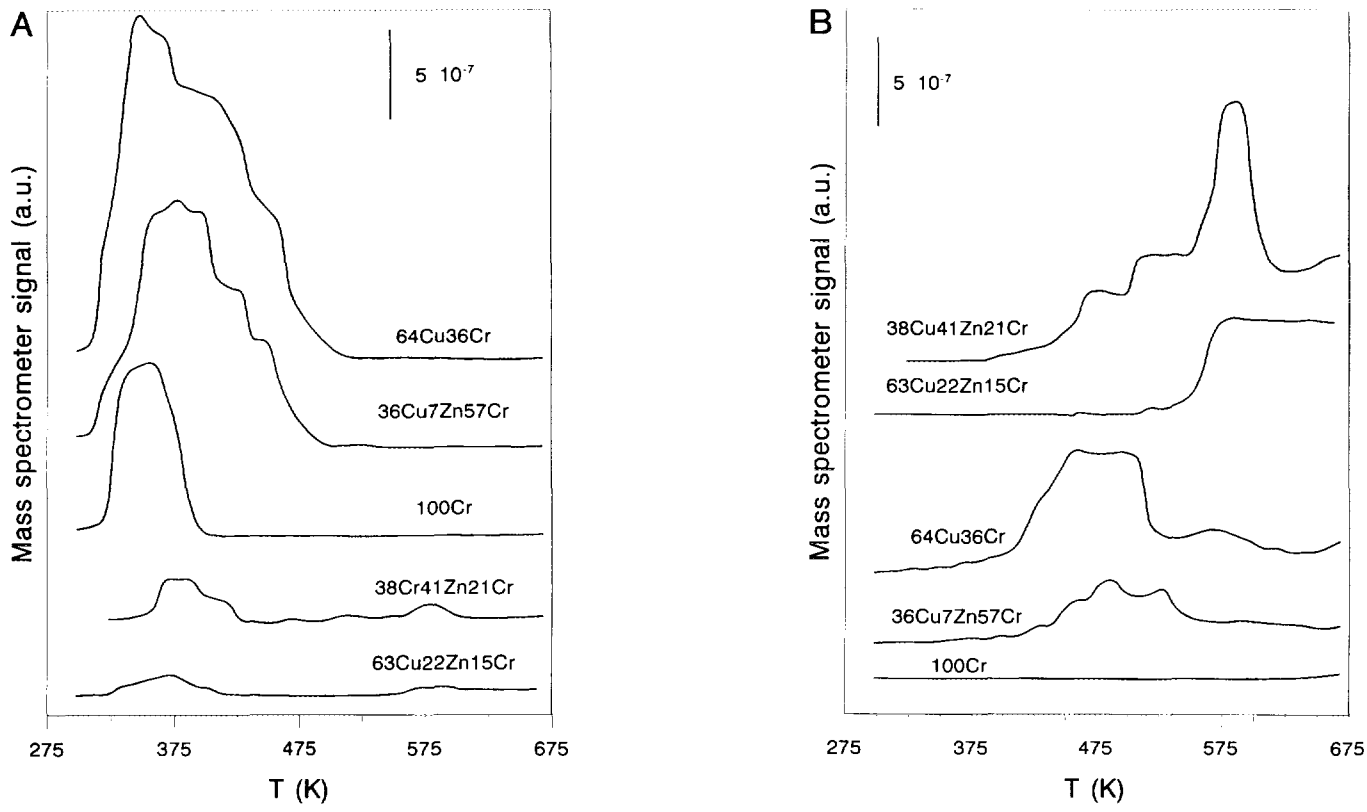

FIG. 2. Temperature-programmed desorption (TPD) profiles for CO (A) and CO_2 (B) after CO chemisorption at room temperature on H_2-reduced catalysts.

catalysts exhibit a notable spinel content as described by XRD.

Photoelectron Spectroscopy

The surface composition of the catalysts and the chemical state of their components have been evaluated by XPS in outgassed and *in situ* H_2-pretreated catalysts at 423, 523, and 623 K. The BEs of the most abundant elements for all samples and pretreatments are summarized in Table 2. Only for the sake of comparison, the Cu $2p_{3/2}$ core level spectra of the two representative catalysts 38Cu41Zn21Cr and 54Cu46Zn, both outgassed and reduced at the three above-mentioned temperatures, are compiled in Figs. 3A and 3B, respectively. From these spectra it is evident that the line profile changes dramatically upon H_2 reduction, in particular at temperatures above 423 K. The outgassed samples display the principal Cu $2p_{3/2}$ peak somewhat above 934.1 eV, which is characteristic of Cu^{2+} species. In several instances, a slight shift towards lower BE of the principal Cu $2p_{3/2}$ peak and the simultaneous observation of two components, the proportions of which depend on the X-ray irradiation time, were observed suggesting some photoreduction of the surface copper oxide layer. An additional means of identifying Cu^{2+} ions is the satellite peak, due to shake-up transitions by ligand → metal 3*d* charge transfer, at ca. 8 eV on the high BE side. Such a transfer cannot occur in Cu_2O and Cu° because of their completely filled 3*d* shells. The disappearance of the satellite peak and the simultaneous shift of the principal Cu $2p_{3/2}$ peak towards lower BE upon H_2 reduction at temperatures above 423 K are conclusive evidence that the copper species are Cu° or Cu^+, but in no case Cu^{2+}. Since the photoelectrons from the core levels and the valence band do not allow differentiation between these species, one has to turn to the X ray induced Cu L_3VV Auger electrons for a clear distinction (48). The modified Auger parameter, $\alpha_{A'}$, is defined by the equation $\alpha_{A'} = h\nu +$ (KE Cu LMM − KE Cu 2 $p_{3/2}$), where the difference in parentheses represents the difference between the kinetic energy of the Cu LMM Auger electron and the Cu $2p_{3/2}$ photoelectron. From the data in Table 2, it is clear that the $\alpha_{A'}$ parameter for CuO and most of the Cu-containing catalysts at values close to or somewhat above 1851 eV for both outgassed and reduced samples corresponds to Cu^{2+} or Cu°. The exceptions are the catalysts with high chromium content in which the $\alpha_{A'}$ parameter is close to or somewhat below 1850 eV, indicative of the presence of Cu^+. The stabilization of such

TABLE 2

Binding Energies of Core Electrons and Auger Parameter of Mixed Oxides Subjected to Various *in situ* Pretreatments

Catalyst	Treatment	BE Cr $2p_{3/2}$	BE Cu $2p_{3/2}$	Auger parameter (eV)
35Cu50Zn15Cr	Vacuum	579.3/576.3	934.1	1852.0
	T_r = 423 K	576.3	933.9	1851.9
	T_r = 523 K	576.0	932.5	1852.0
	T_r = 623 K	576.3	932.3	1851.5
64Cu21Zn15Cr	Vacuum	578.8/575.1	935.4/933.7	1851.8
	T_r = 423 K	575.2	934.6/933.6	1851.7
	T_r = 523 K	575.6	934.1/932.6	1851.6
	T_r = 623 K	575.6	932.5	1851.7
55Cu8Zn37Cr	Vacuum	579.9/576.4	935.1/933.1	1850.5
	T_r = 423 K	576.1	932.8	1851.5
	T_r = 523 K	576.4	932.8	1851.5
	T_r = 623 K	576.3	932.7	1851.5
38Cu41Zn21Cr	Vacuum	579.0/575.2	935.8/933.7	1851.7
	T_r = 423 K	576.7	934.2	1851.5
	T_r = 523 K	576.7	932.5	1851.4
	T_r = 623 K	576.5	932.5	1851.1
60Cu10Zn30Cr	Vacuum	579.3/576.3	935.1/933.5	1850.8
	T_r = 423 K	576.5	935.3/933.6	1850.9
	T_r = 523 K	576.4	935.3/933.6	1851.5
	T_r = 623 K	576.5	932.8	1851.5
36Cu7Zn57Cr	Vacuum	579.4/576.3	935.3/933.1	1850.4
	T_r = 423 K	576.6	935.3/933.3	1850.6
	T_r = 523 K	576.6	932.9/931.1	1851.4/1849.6
	T_r = 623 K	576.7	932.9/931.6	1851.6/1850.3
54Cu46Zn	Vacuum	—	933.8	1852.0
	T_r = 423 K	—	933.8	1851.4
	T_r = 523 K	—	932.5	1851.6
	T_r = 623 K	—	932.5	1851.6
64Cu36Cr	Vacuum	579.3/575.8	934.9/933.0	1850.6
	T_r = 423 K	576.0	935.0/933.0	1850.7
	T_r = 523 K	576.9	932.8/931.3	1851.6/1850.1
	T_r = 623 K	576.9	932.7	1851.4
35Cu50Zn15CrB	Vacuum	579.2/576.7	934.1	1851.5
	T_r = 423 K	576.8	934.2	1851.3
	T_r = 523 K	576.9	932.6	1851.2
	T_r = 623 K	576.4	932.6	1851.4
64Cu21Zn15CrB	Vacuum	576.6	934.8/933.1	1851.8
	T_r = 423 K	576.4	934.8/933.1	1850.9
	T_r = 523 K	576.6	932.4	1851.5
	T_r = 623 K	576.3	932.4	1851.6
55Cu8Zn37CrB	Vacuum	579.1/576.4	934.6	1851.9
	T_r = 423 K	576.4	934.5	1851.9
	T_r = 523 K	576.7	933.2/932.1	1851.5/1850.4
	T_r = 623 K	576.5	932.9/931.7	1851.5/1850.3

a species in a Cu chromite by solid state reaction is consistent with the TPR results, which showed long extending tails at high temperatures of reduction (cf. Fig. 1).

Finally, the binding energy of the Zn $2p_{3/2}$ peak was essentially constant irrespective of sample composition and pretreatments. Accordingly, accurate BE values could also be calculated by taking the Zn $2p_{3/2}$ value as an internal standard. Moreover, rather high BE values were observed for the Cr $2p_{3/2}$ peak in calcined samples, suggesting than surface Cr^{6+} was formed during calcination. However, reduc-

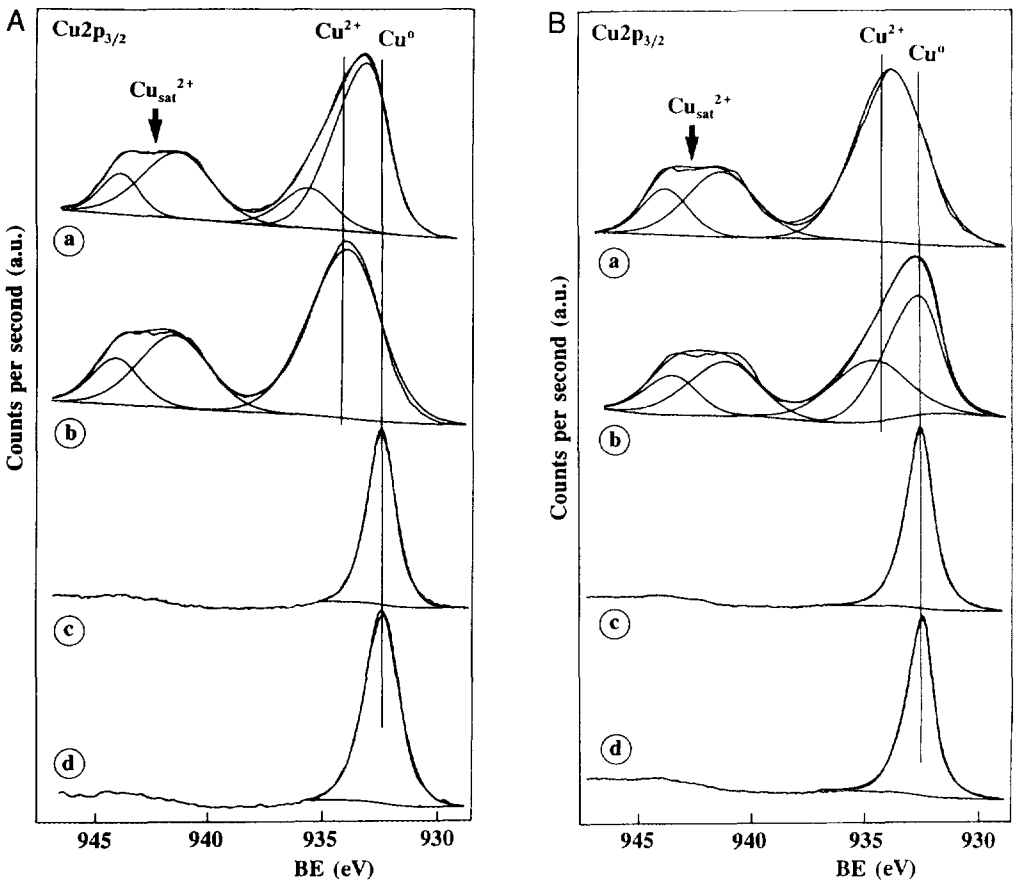

FIG. 3. Cu $2p_{3/2}$ core level spectra for 38Cu41Zn21Cr (A) and 54Cu46Zn (B) representative catalysts subject to different pretreatments: (a) outgassed under vacuum at room temperature; (b), (c), and (d) reduced in hydrogen at 423, 523, and 623 K within the spectrometer pretreatment chamber.

tion in hydrogen under mild conditions, i.e., 423 K, is enough to remove Cr^{6+}, generating exclusively Cr^{3+} species.

From peak areas, photoelectron cross sections, and mean free paths, the Cu/Zn atomic ratios have been calculated (49). The change in this ratio brought about by the reduction temperature is illustrative because it allows one to monitor the sintering of copper particles. The influence of the reduction temperature on the XPS Cu/Zn ratio is displayed in Fig. 4 for three ternary catalysts and compared with that of the Cr-free catalyst 54Cu46Zn. The decrease in Cu/Zn ratio with increased temperature of reduction is clearly visible for all samples, presumably because little Cu surface is exposed for photoelectron emission; however, in the temperature window at which CO hydrogenation is operative the Cu/Zn ratio for the ternary catalysts is almost twice that for the Cr-free counterpart. This result supports the general belief that chromium oxide is a structural promoter (9, 12, 14) which retards sintering of copper by thermal effects.

Relevant chemical information on the nature of surface oxygen species can also be revealed by XPS. After curve fitting procedures, all catalysts displayed two O 1*s* component peaks at ca. 529.9 and 531.7 eV, assigned to O^{2-} lattice and OH^- species, respectively. The OH^-/O^{2-} ratio has been calculated for all the catalysts and pretreatments (see Table 2). In general, the relative surface concentration of hydroxyl groups for the catalysts increases with the temperature of reduction, reaching maxima at ca. 500 K and then decreasing at higher temperatures. This effect can be explained in terms of surface hydroxylation as a result of the reaction between water molecules generated in the reduction process of CuO (and Cu chromite). Only when temperatures are high enough, typically above 500 K, are the surface OHs thermally decomposed into water molecules. Even considering that the desorption process is much more stringent within the XPS spectrometer than in the catalytic reactor, it can be concluded from these results that an important fraction of the catalyst surface is covered by hydroxyl groups, mainly at the lower reaction temperatures.

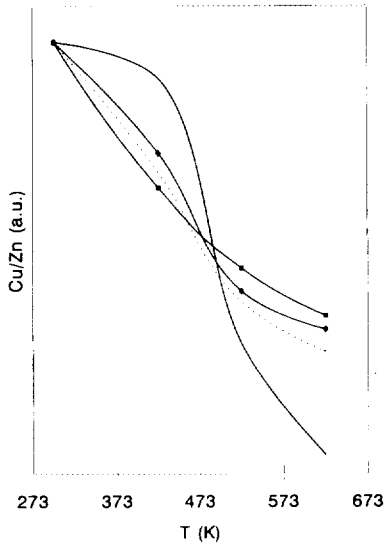

FIG. 4. Influence of the temperature of reduction on the surface (XPS) Cu/Zn atomic ratios for several catalysts: (———) 54Cu46Zn, (···) 63Cu22Zn15Cr, (—◆—) 38Cu41Zn21Cr, (—■—) 36Cu7Zn57Cr.

Activity Measurements

Stationary state activity data were taken at reaction temperatures of 523, 548, 573, and 598 K. The relationship between the reaction temperature and the specific activities shown in Fig. 5 is not straightforward. In principle, the specific activity increases with increasing temperature, reaches a maximum at intermediate temperatures and then decreases at the highest reaction temperatures. The activity decreases at the highest temperatures may be associated with the parallel decrease of exposed copper surface by sintering of metal particles under the severe reducing atmosphere imposed by the H_2/CO mixture in the feed and the overall high pressure in the reactor. In favor of this explanation are the Cu/Zn XPS ratios of H_2-reduced catalysts (Fig. 4) which decreased markedly above 400 K.

The temperature at which the maximum activity is attained depends on the catalyst composition and seems to be associated with the reduction temperature observed on the TPR profiles. For instance, for the catalysts with the lowest onset temperature for reduction, the maximum specific activity also occurs at lower reaction temperatures. Consistently, the sintering of copper particles may well occur first on those catalysts which are reduced at lower temperatures. As pointed out in the section on TPR (Fig. 1), the presence of ZnO in the catalysts plays a key role in the stabilization of copper particles under the reaction conditions (Fig. 4), thus maintaining its active surface. The single-component catalysts, i.e., CuO, ZnO, and Cr_2O_3, are not included in Fig. 5 because of their extremely low activity under the experimental conditions used in this work. Moreover, the catalyst calcined at low temperature have only been tested at the two lowest temperatures (523 and 548 K) but, still displaying a higher surface area, they show a similar activity and a similar variation of activity with temperature than their homologues calcined at higher temperatures.

Selectivity results of CO hydrogenation are compiled in Tables 3 and 4. On all the catalysts and at the different reaction temperatures, the major product is methanol. Moreover, in agreement with literature reports (13, 14), both HAS and hydrocarbon selectivities increase and methanol selectivity decreases with increasing reaction temperature. The HAS selectivities for all the catalysts are shown in Fig. 6. The selectivity to higher alcohols is favored in the Zn-rich compositions whereas chromium contents are needed only in low proportions. As both the Auger parameter of copper and the observation of CO_2 in the TPD spectra of CO chemisorbed on reduced catalysts point to the formation of small Cu° crystallites, it is inferred that in this composition range metallic copper well-dispersed or interacting on the ZnO active surface constitutes the active sites for HAS formation. The strong interaction of CO at the ZnO surface leads to generation of oxygen vacancies at the ZnO surface. These vacancies increase its basic character which appears to stabilize a C_1 oxygenated intermediate species under the reaction conditions, which reacts with a C_n (n = 1, 2, . . .) aldehyde or ketone to form keto-alkoxide. Upon hydrogenation this releases water and is further hydrogenated to the C_{n+1} alcohol product (50, 51). In fact the HAS yield is much higher for the catalysts 38Cu41Zn21Cr and 63Cu22Zn15Cr than for the binary 64Cu36Cr and ternary 36Cu7Zn57Cr counterparts. Therefore, it is tempting to suggest that the ability of a given catalyst to generate oxygen vacancies on the ZnO surface with the subsequent formation of CO_2 can be related with

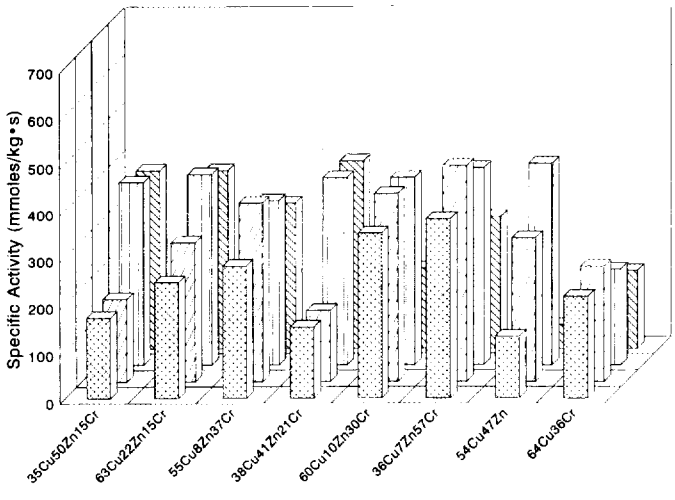

FIG. 5. Specific activities (mmol of CO total converted/kg_{cat} · s) of the catalysts under HAS conditions at four different reaction temperatures: (▨) 523 K, (▨) 548 K, (▨) 573 K, (▨) 598 K.

TABLE 3

Steady State Selectivities and Conversions (Free of CO_2) in CO Hydrogenation (H_2/CO = 0.45 and P = 50 bar) for Catalysts Calcined at 673 K at Different Reaction Temperatures

Catalysts	T (K)	Selectivity (% based on C atoms)					% Conv. CO
		HC	CH_3OH	$C_{2+}OH$	DME	Others	
35Cu50Zn15Cr	523	0	100	0	0	0	7.0
	548	0	96.9	2.8	0.3	0	7.5
	573	3.0	91.9	3.2	0.2	0	7.3
	598	9.7	74.8	10.7	0.1	1.6	6.4
63Cu22Zn15Cr	523	0	99.2	0.5	0.3	0	9.0
	548	0.3	97.0	2.4	0.6	0.7	11.5
	573	1.3	88.4	9.7	2.4	1.1	13.2
	598	5.6	70.1	18.2	3.3	3.2	10.5
55Cu8Zn37Cr	523	0	100	0	0	0	11.3
	548	1.4	93.9	1.0	3.8	0	15.0
	573	4.7	88.5	1.9	4.9	0	13.7
	598	14.4	72.4	5.6	7.5	0.1	12.6
38Cu41Zn21Cr	523	0	98.2	1.5	0	0.3	5.8
	548	6.7	83.4	8.6	0	1.3	6.6
	573	15.7	65.1	15.7	0.7	2.8	12.7
	598	25.8	47.2	20.5	1.4	4.1	13.8
64Cu36Cr	523	0	94.8	0	5.0	0.2	8.4
	548	0	92.6	1.4	5.8	0.2	9.6
	573	3.9	83.3	3.5	8.5	0.8	8.1
	598	12.8	62.2	6.5	17.8	0.7	6.4

Note. HC, hydrocarbons; $C_{2+}OH$, higher alcohols (ethanol, 1-propanol, and isobutanol); DME, dimethyl ether; "Others" are aldehydes, ketones, and esters.

its selectivity to HAS. The increase in HAS selectivity is simultaneous with an increase in ester production (especially methyl esters) (Table 3). Taking into account that the esters arise from the coupling reaction of aldehyde species with surface alkoxide species (52), it is possible to speculate on whether the equilibrium alcohol-aldehyde over the catalyst surface could take place in reaction conditions, indicating that higher alcohols are intermediate in the ester formation. Moreover, it can be observed (Table 3) that Cr-rich catalysts and low-zinc contents give high selectivity to ethers (DME). This effect could be explained considering the acid character of chromium

TABLE 4

Steady State Selectivities and Conversions (Free of CO_2) in CO Hydrogenation (H_2/CO = 0.45 and P = 50 bar) for Catalysts Calcined at 553 K at Different Reaction Temperatures

Catalysts	T (K)	Selectivity (% based on C atoms)					% Conv. CO
		HC	CH_3OH	$C_{2+}OH$	DME	Others	
35Cu50Zn15CrB	523	11.2	82.2	4.3	2.1	0.2	1.0
	548	21.5	41.4	27.5	3.1	1.5	5.2
63Cu22Zn15CrB	523	0	94.0	0.6	4.4	1.0	6.6
	548	0.7	90.9	3.8	4.2	0.4	9.6
55Cu8Zn37CrB	523	3.9	84.2	3.5	7.2	1.2	5.8
	548	7.8	74.0	10.5	6.0	1.8	9.2

Note. HC, hydrocarbons; $C_{2+}OH$, higher alcohols (ethanol, 1-propanol, and isobutanol); DME, dimethyl ether; "Others" are aldehydes, ketones, and esters.

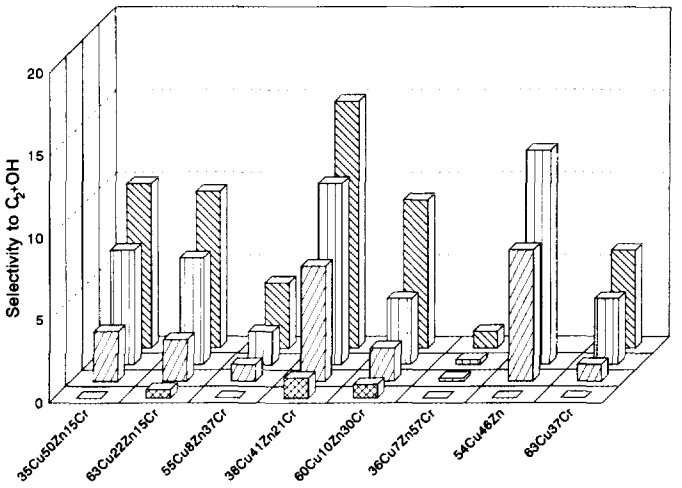

FIG. 6. Higher alcohol (C_2+OH) selectivities (% C) of total of products on the catalysts calcined at 673 K at four different reaction temperatures: (▩) 523 K, (▨) 548 K, (▥) 573 K, (▧) 598 K.

oxide which favours dimethylether (DME) formation from methanol.

On the other hand, as shown in Fig. 7. low calcination temperatures (Catalysts denoted by B at the end) induce increased HAS selectivities in comparison with the respective counterparts calcined at higher temperatures. This particular behaviour may be explained in terms of two alternate explanations. The first is based on the assumption that a less crystalline material develops a larger concentration of copper crystals interacting on the ZnO surface. Line broadening analysis of copper diffraction lines in the XRD patterns of the catalysts after use on-stream demonstrated clearly that the samples calcined at high temperatures show very narrow diffraction peaks, whereas those calcined at low temperatures display broad and diffuse diffraction peaks. The second explanation is more physical in nature. As the catalysts calcined at lower temperatures exhibit substantially higher surface areas and porous structure, transport limitations of the methanol product within the pores may well be operative under the experimental conditions (53), which would favour formation of higher alcohols. A comparison of Tables 3 and 4 (catalysts calcined at 673 and 553 K) shows that catalysts calcined at low temperatures have higher selectivity to DME. This fact can be attributed to a decrease in surface acidity when samples were calcined at 673 K, probably induced by solid state reaction, which inhibits the chromium oxide acidity.

CONCLUSION

The ternary system Cu–Zn–Cr gives useful catalysts for the production of higher alcohols from syngas. The composition was found to be very critical on both activity and HAS selectivity. As chromia does not seem to participate in the catalytic sites, its beneficial effect, even in small amounts, can be understood in terms of a structural promoter because it increases the BET area of the catalysts and also inhibits the sintering of copper particles. Moreover, as revealed by XPS and XRD, the Cr-rich catalysts develop a $CuCr_2O_4$ spinel. The role of chromium in the catalyst formulation can be sumarized as follows: (i) to decrease the onset temperature for the reduction of segregated copper oxide; (ii) to stabilize partially oxidized copper in the reduced catalysts, the Cu(I) species being detected by XPS only in those catalysts in which $CuCr_2O_4$ was present in calcined catalysts; (iii) to stabilize catalyst activity, in particular at higher reaction temperatures; (iv) to increase surface acidity when present at high loadings, which is relected in an increase in DME selectivity.

Copper oxide interacts strongly with the zinc oxide, as evidenced by the shift of TPR profiles toward higher temperatures of reduction with respect to that of the pure CuO counterpart. Such a requirement seems to play a key role in the formation of higher alcohols as the best selectivities to HAS were found in the low Cr content compositions. In addition to this, the CO chemisorbed on the low Cr content catalysts is essentially desorbed as CO_2. This property may be related to the ability of the catalysts to generate oxygen vacancies on the ZnO surface in the presence of gaseous CO. Accordingly, such an ability might well be connected, in a first approximation, with the selectivity to produce higher alcohols by reaction of generated C_1 oxygenated intermediate species stabilized on ZnO with C_n aldehyde or ketone intermediates.

Low calcination temperatures yield poorly crystallized

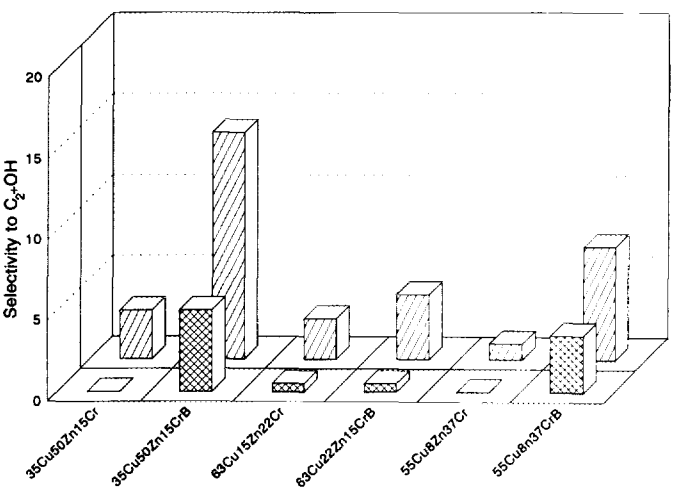

FIG. 7. Comparison of HAS selectivities (% C) of total of products on catalysts calcined at 673 K and 553 K at two different reaction temperatures: (▩) 523 K, (▨) 548 K.

catalysts. These catalysts are reduced at higher temperatures than the homologues calcined at 673 K and display high selectivities to higher alcohols. This effect may be explained on the basis of chemical and physical arguments. On the one hand, the amorphous structure of the catalysts may favour the interaction of small copper particles with the zinc oxide surface, thus increasing the proportion of the active sites. On the other, as these catalysts develop a porous structure diffusional control of the methanol molecules produced within the catalyst pores towards the outer catalyst surface is expected to occur, thus increasing the chain growth probability.

ACKNOWLEDGMENTS

The authors express their gratitude to the CICYT (Spain) for supporting this research (Grant MAT91-0494). They are also indebted to Prof. K. Klier, Department of Chemistry, Lehigh University, for critical reading of this manuscript.

REFERENCES

1. Hindermann, J. P., Hutchings, G. J., and Kiennemann, A., *Catal. Rev. Sci. Eng.* **35**(1), 1 (1993).
2. Solymosi, F., *Catal. Rev.* **1,** 233 (1968).
3. Smith, J. R., Arlington, F. J., and Gay, J. G., *Phys. Rev. B* **26,** 1072 (1982).
4. Sachtler, W. M. H., *in* "Proceedings of the 10th Iberoamerican Symposium on Catalysis, Mérida, Venezuela, 1986," Vol. 2, p. 1327.
5. Industrial Chemistry Library, "C1 Chemistry in Japan," Vol. 1, p. 145. Elsevier, Amsterdam, 1989.
6. Courty, Ph., and Chaumette, P., "Heterogeneous Catalysts for Carbon Monoxide Conversion." NATO Workshop, Newport, 1988.
7. Fox, J. M., *Catal. Rev. Sci. Eng.* **35,** 169 (1993).
8. Kung, H. H., *Catal. Rev. Sci. Eng.* **22,** 235 (1980).
9. Klier, K., *Adv. Catal.* **31,** 243 (1982).
10. Bart, J. C. J., and Sneeden, R. P. A., *Catal. Today* **2,** 1 (1987).
11. Xiaoding, Xu, Doesburg, E. B. M., and Scholten, J. J. F., *Catal. Today* **2,** 125 (1987).
12. Chinchen, G. C., Denny, P. J., Jennings, J. R., Spencer, M. S., and Waugh, K. C., *Appl. Catal.* **36,** 1 (1988).
13. Forzatti, P., Tronconi, E., and Pasquon, I., *Catal. Rev. Sci. Eng.* **33,** 109 (1991).
14. Slaa, J. C., van Ommen, J. G., and Ross, J. R. H., *Catal. Today* **15,** 243 (1992).
15. Rostrup-Nielsen, J. R., *in* "Catalysis-Science and Technology" (J. R. Anderson and M. Boudart, Eds.), Vol. 5. Springer-Verlag, Berlin/New York, 1984.
16. Wender, I., *Catal. Rev. Sci. Eng.* **14,** 97 (1976).
17. Courty, Ph., Chaumette, P., Raimbault, C., and Travers, Ph., *Rev. Int. Fr. Petrole* **45,** 561 (1987).
18. Guibet, J. C., *Pet. Tech.* **335,** 5 (1987).
19. Mintz, M. S., and Quaderer, G. J., "Alcohol as an Octane Enhancer" (Alcohol Week). San Antonio, TX 1985.
20. Liu, L., Wang, H., Fu, J., Li, Y., and Tsui, K., "Proceedings, 9th International Congress on Catalysis, Calgary, 1988" (M. J. Phillips and M. Ternan, Eds.) Vol. 2, p. 735. Chem. Institute of Canada, Ottawa, 1988.
21. Gray, C. L., and Alson, J. A., *Sci. Am.* **86** (1989).
22. Kuirun, P., Hua, Z., Xuecheng, C., Zexeng, Z., and Pengja, L., *in* "7th International Symposium on Alcohol Fuels, Paris, 1986." Technip, Paris, 1986.
23. Slocum, P. J., "California Fuel Methanol Cost Study," presented at the Economics Workshop–California Advisory Board on Air Quality and Fuels, San Francisco, February 1–2, 1989.
24. Hiller, H., and Supp, E., *Erdoel Kohle. Erdgas. Petrochem.* **38,** 14 (1985).
25. Burch, R., Golunski, S. E., and Spencer, M. S., *J. Chem. Soc. Faraday Trans.* **86,** 2683 (1990).
26. Robbins, J. L., Iglesia, E., Kelkar, C. P., and deRite, B., *Catal. Lett.* **10,** 1 (1990).
27. Chinchen, G. C., Denny, P. J., Parker, D. G., Short, G. D., Spencer, M. S., Waugh, K. C., and Whan, D. A., *Prepr. Am. Chem. Soc. Div. Fuel Chem.* **29,** 178 (1984).
28. Chinchen, G. C., Waugh, K. C., and Whan, D. A., *Appl. Catal.* **25,** 101 (1986).
29. Burch, R., Golunski, S. E., and Spencer, M. S., *Catal. Lett.* **6,** 152 (1990).
30. Herman, R. G., Klier, K., Simmons, G. W., Finn, B. P., Bulko, J. B., and Kobylinski, T. P., *J. Catal.* **56,** 407 (1979).
31. Nomeman, L. E. Y., and Ponec, V., *Catal. Lett.* **7,** 213 (1990).
32. Ponec, V., *Catal. Lett.* **11,** 249 (1991).
33. Szanyi, J., and Goodman, D. W., *Catal. Lett.* **10,** 383 (1991).
34. Fleisch, T. H., and Mieville, R. L., *J. Catal.* **90,** 165 (1984).
35. Clausen, B. S., Lengeler, R. L., Rasmunsen, B. S., and Topsøe, H., "Proceedings, International Congress Prog. X-Ray Studies by Synchroton Radiation, Strasbourg, 1985," paper 2.
36. Fleisch, T. H., and Mieville, R. L., *J. Catal.* **97,** 284 (1987).
37. Sankar, G., Vasudevan, S., and Rao, C. N. R., *J. Chem. Phys.* **85,** 2291 (1986).
38. Kau, L-S, Hogson, K. O., and Solomon, E. I., *J. Am. Chem. Soc.* **111,** 7103 (1989).
39. Arunarkavalli, T., Kulkarni, G. U., and Rao, C. N. R., *Catal. Lett.* **20,** 259 (1993).
40. Nunan, J. G., Bogdan, C. E., Klier, K., Smith, K. J., Young, C-W, and Herman, R. G., *J. Catal.* **113,** 410 (1988).
41. Smith, K. J., Young, C-W, Herman, R. G., and Klier, K., *Solid State Chem. Catal.* ACS Symposium Series, Vol. 279, Am. Chem. Soc., Washington, DC, 1985.
42. Shiskov, D. S., Stravrakeva, D. A., and Kasabova, N. A., *Kinet. Katal.* **21,** 1559 (1980).
43. Boyce, A. L., Graville, S. R., Sermon, P. A., and Vong, M. S. W., *React. Kinet. Catal. Lett.* **44,** 1 (1991).
44. Boyce, A. L., Graville, S. R., Sermon, P. A., and Vong, M. S. W., *React. Kinet. Catal. Lett.* **44,** 13 (1991).
45. Vong, M. S. W., Sermon, P. A., and Grant, K., *Catal. Lett.* **4,** 15 (1990).
46. Boyce, A. L., Sermon, P. A., Vong, M. S. W., and Yates, M. A., *React. Kinet. Catal. Lett.* **44,** 309 (1991).
47. Waugh, K. C., *Catal. Today.* **18,** 147 (1993).
48. See, for instance, Fierro, J. L. G., *in* "Properties and Applications of Perovskite-Type Oxides" (L. G. Tejuca and J. L. G. Fierro, Eds.), Chap. 12, p. 255. Dekker, New York, 1993.
49. "Practical Surface Analysis. Auger and X-ray Photoelectron Spectroscopy" (D. Briggs and M. P. Seah, Eds.), 2nd ed., Wiley, Chichester, 1990.
50. Nunan, J. G., Bogdan, C. E., Klier, K., Smith, J., Young, C.-W., and Herman, R. G., *J. Catal.* **116,** 195 (1989).
51. Nunan, J. G., Herman, R. G., and Klier, K., *J. Catal.* **116,** 222 (1989).
52. Vedage, G. A., Himelfarb, P. B., Simmons, G. W., and Klier, K., *ACS Symp. Ser.* **279,** 295 (1985).
53. Berndt, H., Briehn, V., Evert, S., Gutschick, D., and Kotowski, W., *Catal. Lett.* **14,** 185 (1992).